Article

Impact of Thermal Radiation and Heat Source/Sink on Eyring–Powell Fluid Flow over an Unsteady Oscillatory Porous Stretching Surface

Abdullah Dawar [1], **Zahir Shah [2],***, **Muhammad Idrees [3]**, **Waris Khan [3]**, **Saeed Islam [2]** and **Taza Gul [4]**

[1]   Department of Mathematics, Qurtuba University of Science and Information Technology, Peshawar 25000, Pakistan; abdullah.mathematician@gmail.com
[2]   Department of Mathematics, Abdul Wali Khan University, Mardan 23200, Pakistan; saeedislam@awkum.edu.pk
[3]   Department of Mathematics, Islamia College, Peshawar 25000, Pakistan; idrees@icp.edu.pk (M.I.); wariskhan758@yahoo.com (W.K.)
[4]   Department of Mathematics, City University of Science and Information Technology, Peshawar 25000, Pakistan; tazagul@cusit.edu.pk
*   Correspondence: zahir1987@gist.edu.pk; Tel.: +92-333-9198-823

check for
updates

Abstract: The main intention of this article is to examine the heat transmission of the flow of Eyring–Powell fluid over an unstable oscillatory porous stretching surface. The effect of thermal radiation on the fluid flow is investigated, where the flow is actuated by the unbounded flexible surface, which is extended occasionally to and fro on its plane. The rudimentary leading equations are changed to differential equations through the use of applicable similarity variables. An optimal and numerical approach was used to find the solution to the modeled problems. The convergence of the homotopy analysis method (HAM) is shown numerically. The homotopy analysis method predictions of the structures formed are in close agreement with the obtained results from the numerical method. Comparisons between HAM and numerical methods are shown graphically as well as numerically. The convergence of this method is shown numerically. The impacts of the skin friction and heat flux are shown through a table. The influence of the porosity, oscillation, thermal radiation, and heat absorption/generation are the main focus of this work. The consequences of emerging parameters are demonstrated through graphs.

Keywords: Eyring–Powell fluid; thermal radiation; porosity; oscillatory stretched sheet; HAM

1. Introduction

Boundary layer fluid flow problems in different dimensions through a stretching sheet with heat transfer and magnetohydrodynamic effects have plentiful and inclusive applications in several engineering and industrial sectors. They include glass blowing melt spinning, heat exchanger design, fiber and wire coating, production of glass fibers, industrialization of rubber and plastic sheets, etc. In addition, the action of thermal radiation is vital to calculating heat transmission in the polymer treating industry. In investigations of all these applications, many investigators deliberate the flow of different fluid models over a stretching sheet. Sakiadis [1] studied boundary layer flow over a flat surface. Crane [2] obtained the closed-form solution for the flow instigated by the stretching of a flexible parallel sheet moving periodically. Gupta and Gupta [3] extended this work by considering suction/blowing at the surface of the sheet. The dissemination of chemically reactive species over a moving continuous sheet was studied by Anderson et al. [4]. Pop [5] studied time-dependent flow

over a stretched surface. The impact of heat transmission on second-grade fluid over a stretching sheet was explored by Cortell et al. [6]. Areal [7] studied an asymmetric viscoelastic fluid flow past a stretching sheet for different purposes in the fluid field. Rashdi et al. [8,9] studied entropy generation in magneto hydrodynamic Eyring–Powell fluid and Carreau nanofluid through a permeable stretching surface. Hayat et al. [10–13] studied boundary layer flow using different phenomena.

There are no solitary constitutive equations for non-Newtonian fluid that clarify all the distinctive aspects of compound rheological fluids. The Eyring–Powell model [14], an important subclass of these, models from the kinetic theory of liquids instead of experimental relations. Recently, Prasad [15] studied heat transfer and momentum in Eyring–Powell fluid over a nonisothermal stretching sheet. Noreen et al. [16] examined the peristaltic flow of magnetohydrodynamic Eyring–Powell fluid in a channel. Ellahi [17] recently completed a numerical study of the magnetohydrodynamic generalized Couette flow of Eyring–Powell fluid with heat transfer and the slip condition. Ellahi et al. [18] examined the shape effects of spherical and nonspherical nanoparticles in mixed convection flow over a vertical stretching permeable sheet. Other related studies concerning Eyring–Powell fluid can be seen in [19–25].

Thermal radiation is the procedure in which energy is released in the form of electromagnetic radiation by a surface in all directions. Thermal radiation has numerous uses in the areas of engineering and heat transfer analysis. In the case of conduction and convection, energy transmission amongst objects depends almost entirely on the temperature. For natural free convection, or when variable property effects are included, the power of the temperature difference may be slightly larger than one, and can reach two. Tawade et al. [26] investigated a thin liquid flow through a stretching surface with the influence of thermal radiation and a magnetic field. A brief discussion was given on physical parameters in his work. Ellahi et al. [27] examined the boundary layer magnetic flow of nano-ferroliquid under the influence of low oscillation over a stretchable rotating disk. Zeeshan et al. [28] studied the effect of a magnetic dipole on viscous ferrofluid past a stretching surface with thermal radiation. The Hall effect on Falkner–Skan boundary layer fluid flow over a stretching sheet was examined by Maqbool et al. [29]. The enhancement of heat transfer and heat exchange effectiveness in a double-pipe heat exchanger filled with porous media was examined by Shirvan et al. [30]. Ramesh et al. [31] studied the Casson fluid flow near the stagnation point over a stretching sheet with variable thickness and radiation. Other related studies concerning stretching sheets can be seen in [32–34]. Bakier and Moradi et al. [35,36] studied the influence of thermal radiation on assorted convective flows on an upright surface in a permeable medium. Chaudhary et al. [37] investigated the thermal radiation effects of fluid on an exponentially extending surface.

The aim of the current research is to investigate the heat transmission of Eyring–Powell fluid over an unsteady oscillatory porous stretching surface. The homotopy analysis method (HAM) was used in the present work for the solution of modelled equations that are nonlinear and coupled. The homotopy analysis method is a substitute method and its main advantage is in its application to nonlinear differential equations without discretization and linearization. In 1992, Liao [38–40] was the first to investigate this technique for the solution of this type of problem and generally proved that this method is rapidly convergent to the approximated solutions. Solutions using this technique are significant because they involve all the physical parameters of the problem and we can easily discuss their behavior. Due to its fast convergence, many researchers [41–44] have used this procedure to solve highly nonlinear combined equations. The effects of all the embedding parameters have been studied graphically. Khan et al. [45] studied the flow and heat transfer of Eyring–Powell fluid over an oscillatory stretching sheet with thermal radiation. Shah et al. [46,47] studied the effects of a Hall current on three-dimensional non-Newtonian nanofluids and micropolar nanofluids in a rotating frame. Hameed et al. [48] investigated the combined magnetohydrodynamic and electric field effect on an unsteady Maxwell nanofluid flow over a stretching surface under the influence of variable heat and thermal radiation. Recently Muhammad et al. [49] studied the rotating flow of magnetohydrodynamic

carbon nanotubes over a stretching sheet with the impact of non-linear thermal radiation and heat generation/absorption.

2. Formulation of the Problem

Consider a two-dimensional incompressible boundary layer flow of Eyring–Powell fluid over an oscillating stretched sheet concurring with plane y (Figure 1). In the Cartesian coordinate system, x is beside the sheet and y is vertical to the sheet. The fluid flow is assumed to be in an unsteady state and the stretching sheet is kept porous. Let T_w denote the surface temperature and T_∞ denote the temperature of the fluid as the distance from the surface tends to infinity. It is assumed that $T_w > T_\infty$. The Cauchy stress tensor for Eyring–Powel fluid [15–25] is

$$\overrightarrow{T} = -\overrightarrow{P}\overrightarrow{I} + \overrightarrow{\tau}_{ij}, \tag{1}$$

where $\overrightarrow{\tau}_{ij}$ for the Eyring–Powel fluid is

$$\overrightarrow{\tau}_{ij} = \mu \frac{\partial \overrightarrow{u}_i}{\partial x_j} + \frac{1}{\alpha}\sinh^{-1}\left(\frac{1}{c}\frac{\partial \overrightarrow{u}_i}{\partial x_j}\right). \tag{2}$$

Here, α and c denote the Eyring–Powel fluid constants. We expand the term $\sinh^{-1}\left(\frac{1}{c}\frac{\partial \overrightarrow{u}_i}{\partial x_j}\right)$ as below:

$$\sinh^{-1}\left(\frac{1}{c}\frac{\partial \overrightarrow{u}_i}{\partial x_j}\right) = \frac{1}{c}\frac{\partial \overrightarrow{u}_i}{\partial x_j} - \frac{1}{6}\left(\frac{1}{c}\frac{\partial \overrightarrow{u}_i}{\partial x_j}\right)^3, \left|\frac{1}{c}\frac{\partial \overrightarrow{u}_i}{\partial x_j}\right| < 1. \tag{3}$$
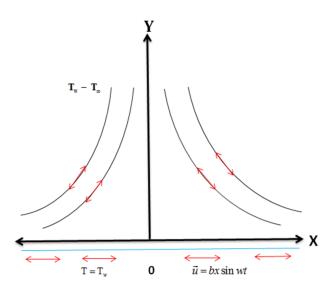

Figure 1. Geometrical figure of the problem.

Using the boundary layer approximations, the continuity, energy equations and momentum are as:

$$\frac{\partial \overrightarrow{u}}{\partial x} + \frac{\partial \overrightarrow{v}}{\partial y} = 0 \tag{4}$$

$$\frac{\partial \overrightarrow{u}}{\partial t} + \overrightarrow{u}\frac{\partial \overrightarrow{u}}{\partial x} + \overrightarrow{v}\frac{\partial \overrightarrow{u}}{\partial y} = \left(v + \frac{1}{\rho\Psi Y}\right)\frac{\partial^2 \overrightarrow{u}}{\partial y^2} - \frac{1}{2\rho\Psi Y^3}\left(\frac{\partial \overrightarrow{u}}{\partial y}\right)^2\frac{\partial^2 \overrightarrow{u}}{\partial y^2} - \frac{v}{k}\overrightarrow{u} \tag{5}$$

$$\rho C_p \left(\left(\frac{\partial T}{\partial t} \right) + \vec{u} \left(\frac{\partial T}{\partial x} \right) + \vec{v} \left(\frac{\partial T}{\partial y} \right) \right) = k \left(\frac{\partial^2 T}{\partial y^2} \right) - \left(\frac{\partial Q_{rad}}{\partial y} \right) + \frac{Q_0}{\rho C_p} (T - T_\infty) \tag{6}$$

The terms $\vec{u}$ and $\vec{v}$ represent the velocity component in the directions of x and y, respectively; v indicates the kinematic viscosity; the symbol ρ denotes the density; Ψ and Y are the fluid materials; C_p indicates the specific heat; Q_0 is the heat source/sink; k signifies thermal conductivity; and Q_{rad} is the radiative heat flux is defined as

$$Q_{rad} = -\frac{4\sigma'}{3k'} \frac{\partial T^4}{\partial y}, \tag{7}$$

where σ' denotes the Stefan–Boltzmann constant and k' is the absorption coefficient.

Expanding Equation (7) by Taylor series, we obtain

$$T^4 = T_\infty{}^4 + 4T_\infty{}^3(T - T_\infty) + 6T_\infty{}^2(T - T_\infty)^2 + \dots \tag{8}$$

By neglecting the higher terms from Equation (8), we get

$$T^4 = 4T_\infty^3 T - 3T_\infty^4. \tag{9}$$

In observation of Equations (7) and (8), Equation (6) becomes

$$\rho C_p \left(\frac{\partial T}{\partial t} + \vec{u} \frac{\partial T}{\partial x} + \vec{v} \frac{\partial T}{\partial y} \right) = \left(k + \frac{16\sigma' T_\infty{}^3}{3k'} \right) \frac{\partial^2 T}{\partial y^2} + \frac{Q_0}{\rho C_p} (T - T_\infty). \tag{10}$$

The subjected boundary condition for the flow phenomena [45] is

$$\vec{u} = \vec{u}_w = bx \sin \omega t, \vec{v} = 0, T = Tw \text{ at } y = 0, t > 0,$$
$$\vec{u} \to 0, T \to T_\infty \text{ at } y \to \infty, \tag{11}$$

where the dimensionless variables are given as

$$y = \sqrt{\frac{b}{v}} y, \ \tau = t\omega, \ \vec{u} = bx F_y(y, \tau), \ \vec{v} = -\sqrt{vb} F(y, \tau), \ G(y, \tau) = \frac{T - T_\infty}{T_w - T_\infty}. \tag{12}$$

In observation of the dimensionless variables defined above, Equations (5) and (10) reduce to

$$(1 + K)F''' - AF'' - (F')^2 + FF'' - \lambda K F''^2 F''' - \kappa F' = 0, \tag{13}$$

$$(1 + Rd)G'' + \Pr(FG' - AG') - \gamma G = 0, \tag{14}$$

with the boundary conditions

$$F'(0, \tau) = \sin \tau, F(0, \tau) = 0, G(0, \tau) = 1, F'(\infty, \tau) = 0, G(\infty, \tau) = 0. \tag{15}$$

In the above equations, $K = \frac{1}{\mu \Psi Y}$ and $\lambda = \frac{x^2 b^3}{2v Y^2}$ are dimensionless material fluid parameters, $\kappa = \frac{v}{kb}$ indicates the porosity, $A = \frac{\omega}{b}$ represents the ratio of the oscillation frequency, $\gamma = \frac{v Q_0}{kb\rho C_p} \left(\frac{T - T_\infty}{T_w - T_\infty} \right)$ represents the heat source/sink, $\Pr = \frac{\mu C_p}{k}$ denotes the Prandtl number, and $Rd = \frac{16\sigma' T_\infty^3 T}{3kk'}$ is the radiation parameter. According to Javed et al. [27], Equation (15) is subject to the constraint $\lambda K << 1$.

Physical Quantities of Interest

The physical quantities for interest to engineers, such as skin friction C_f and the local Nusselt number Nu_x, are defined as

$$C_f = \frac{\tau_w}{\rho u_w^2}, \; Nu_x = \frac{xq_w}{k(T_w - T_\infty)}, \; q_w = -k\left(\frac{\partial T}{\partial y}\right)_{y=0},$$
(16)

In observation of Equation (12), Equation (16) takes the following forms:

$$\text{Re}_x^{\frac{1}{2}} Cf = (1+K)F'' - \frac{K}{3}\Psi(F''(0)), \text{Re}_x^{\frac{1}{2}} Nu_x = -\left(1 + \frac{4}{3}Rd\right)G'(0).$$
(17)

3. Solution by HAM

Liao was the first person who used the basic idea of a topology called homotopy and derived a new method known as the homotopy analysis method. He used two homotopic functions to derive this technique. Two functions are called homotopic functions when one of them can be continuously distorted into the other. Let H_1, H_2 be two functions that are continuous and X_1, X_2 be two topological spaces where H_1 and H_2 map from X_1 to X_2; then H_1 is said to be homotopic to H_2 if there is a continuous function $\overline{f}$,

$$\overline{f} : X_1 \times [0, 1] \to X_2,$$
(18)

such that, $\forall \, x \in X_1$,

$$\overline{f}[x, 0] = H_1(x) \text{ and } \overline{f}[x, 0] = H_2(x).$$
(19)

This mapping $\overline{f}$ is then called homotopic.

In order to solve Equations (13) and (14) with the boundary Condition (15), we use the HAM according to the following process. The preliminary guesses are

$$F_0(\Gamma) = 1 - e^{-\Gamma}\sin\Gamma, \; G_0(\Gamma) = e^{-\Gamma}.$$
(20)

The linear operators are taken as L_F and L_G :

$$L_F(F) = F''' - F', \; \text{L}_G(G) = G'' - G.$$
(21)

These operators have the following properties:

$$L_F(\psi_1 + \psi_2 e^{-\Gamma} + \psi_3 e^{\Gamma}) = 0, \; \text{L}_G(\psi_4 e^{-\Gamma} + \psi_5 e^{\Gamma}) = 0,$$
(22)

where $\psi_i(i = 1 - 5)$ are constants.

The nonlinear operators N_F and N_G are specified as

$$\begin{aligned} \text{N}_\text{F}[F(\Gamma;\mho)] &= (1+K)\frac{\partial^3 F(\Gamma;\mho)}{\partial\Gamma^3} - A\frac{\partial^2 F(\Gamma;\mho)}{\partial\Gamma^2} - \left(\frac{\partial F(\Gamma;\mho)}{\partial\Gamma}\right)^2 \\ &- \lambda k\left(\frac{\partial^2 F(\Gamma;\mho)}{\partial\Gamma^2}\right)^2 \frac{\partial^3 F(\Gamma;\mho)}{\partial\Gamma^3} - \kappa\frac{\partial F(\Gamma;\mho)}{\partial\Gamma}, \end{aligned}$$
(23)

$$(1+Rd)\frac{\partial^2 G(\Gamma;\mho)}{\partial\Gamma^2} + \text{Pr}\left(F(\Gamma;\mho)\frac{\partial G(\Gamma;\mho)}{\partial\Gamma} - A\frac{\partial G(\Gamma;\mho)}{\partial\Gamma}\right) - \gamma G(\Gamma;\mho) = 0.$$
(24)

The zero-order problems from Equations (13) and (14) are

$$\begin{aligned} (1-\mho)\text{L}_\text{F}[F(\Gamma;\mho) - F_0(\Gamma)] &= \hbar_\text{F}\text{N}_\text{F}[F(\Gamma;\mho)], \\ (1-\mho)\text{L}_\text{G}[G(\Gamma;\mho) - G_0(\Gamma)] &= \hbar_\text{G}\text{N}_\text{G}[F(\Gamma;\mho), G(\Gamma;\mho)]. \end{aligned}$$
(25)

The equivalent boundary conditions are

$$
\begin{aligned}
&F(\Gamma;\mho)\big|_{\Gamma=0}=0,\ \frac{\partial F(\Gamma;\mho)}{\partial\Gamma}\bigg|_{\Gamma=0}=\sin\tau,\ \frac{\partial F(\Gamma;\mho)}{\partial\Gamma}\bigg|_{\Gamma=\to\infty}=0,\\
&G(\Gamma;\mho)\big|_{\Gamma=0}=1,\ G(\Gamma;\mho)\big|_{\Gamma\to\infty}=0,
\end{aligned}
\tag{26}
$$

where $0\le\mho\le1$ is the embedding parameter. When $\mho=0$ and $\mho=1$, we have

$$
F(\Gamma;1)=F(\Gamma)\ \text{and}\ G(\Gamma;1)=G(\Gamma).
\tag{27}
$$

Expanding $F(\Gamma;\mho)$ and $G(\Gamma;\mho)$ by Taylor series,

$$
\begin{aligned}
F(\Gamma;\mho)&=F_0(\Gamma)+\sum_{q=1}^{\infty}F_q(\Gamma)^q\\
G(\Gamma;\mho)&=G_0(\Gamma)+\sum_{q=1}^{\infty}G_q(\Gamma)^q
\end{aligned}
\tag{28}
$$

where

$$
F_q(\Gamma)=\frac{1}{q!}\frac{\partial F(\Gamma;\mho)}{\partial\Gamma}\bigg|_{=0}\ \text{and}\ G_q(\Gamma)=\frac{1}{q!}\frac{\partial G(\Gamma;\mho)}{\partial\Gamma}\bigg|_{=0}.
\tag{29}
$$

Setting $\mho=1$ in (29), we obtain

$$
\begin{aligned}
F(\Gamma)&=F_0(\Gamma)+\sum_{q=1}^{\infty}F_q(\Gamma),\\
G(\Gamma)&=G_0(\Gamma)+\sum_{q=1}^{\infty}G_q(\Gamma).
\end{aligned}
\tag{30}
$$

The qth-order problem satisfies the following:

$$
\begin{aligned}
L_F\big[F_q(\Gamma)-\chi_q F_{q-1}(\Gamma)\big]&=\hbar_F U_q^F(\Gamma)\\
L_G\big[G_q(\Gamma)-\chi_q G_{q-1}(\Gamma)\big]&=\hbar_G U_q^G(\Gamma)
\end{aligned}
\tag{31}
$$

with the conditions

$$
\begin{aligned}
F_q(0)&=F_q'(0)=F_q'(\infty)=0,\\
G_q(0)&=G_q(\infty)=0.
\end{aligned}
\tag{32}
$$

Here,

$$
U_q^F(\Gamma)=(1+K)F_{q-1}'''-AF_{q-1}''-\sum_{k=0}^{q-1}F_{q-1-k}'F_k'+\sum_{k=0}^{q-1}F_{q-1-k}F_k''-\lambda k\sum_{k=0}^{q-1}F_{q-1-k}''\sum_{j=0}^{k}F_{k-j}''F_j'''-\kappa F_{q-1}'
\tag{33}
$$

$$
U_q^G(\Gamma)=(1+Rd)G_{q-1}''+\Pr\left[\sum_{k=0}^{q-1}F_{q-1-k}G_k'-AG_{q-1}'\right]-\gamma G_{q-1}
\tag{34}
$$

where

$$
\chi_q=\begin{cases}0,&\text{if }\le1\\1,&\text{if }>1\end{cases}
\tag{35}
$$

4. HAM Solution Convergence

When we compute the series solutions of the velocity and temperature functions in order to use HAM, the assisting parameters h_f, h_θ appear. These assisting parameters are responsible for adjusting the convergence of these solutions. The $\hbar$-curves of $f''(0)$ and $\theta'(0)$, at 12th-order approximations are plotted in Figures 2 and 3 for dissimilar values of the embedding parameter. The $\hbar$-curves consecutively display the valid region.
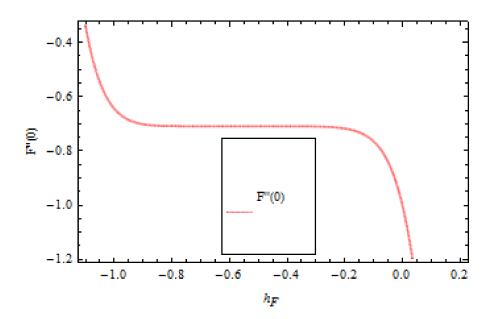
Figure 2. The $\hbar$-curve graph of velocity profile, when $Pr = 0.5$, $K = 0.5$, $Rd = 0.5$, $\lambda = 0.5$, $\kappa = 0.5$, $\gamma = 0.5$, $\operatorname{Sin}\tau = 1.0$, $A = 0.5$.
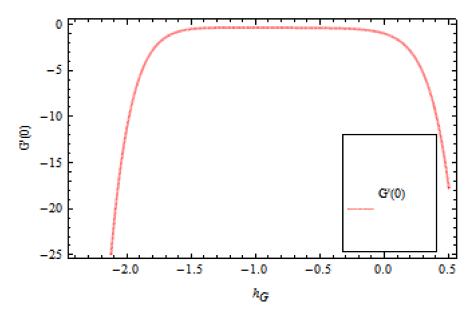

Figure 3. The $\hbar$-curve graph of temperature profile, when $Pr = 0.5$, $K = 0.5$, $Rd = 0.5$, $\lambda = 0.5$, $\kappa = 0.5$, $\gamma = 0.5$, $\operatorname{Sin}\tau = 1.0$, $A = 0.5$.

5. Results and Discussion

In this section, we present the special effects of the concerned parameters graphically. In all the graphs, the values of K and λ are chosen such that the product λK should be much smaller than one. Figure 4 shows the effect of the rate of the relative amplitude of frequency and the stretching rate A on the time series of the velocity distribution. It is observed that the amplitude of the flow motion falls with large values of A. Figure 5 demonstrates the effect of A on the temperature profile. It is observed that the temperature profile G decreases as A increases. Actually, the amplitude of oscillation rises for large values of A which, in turn, decreases the temperature. The influence of the Prandtl number (Pr) on the temperature distribution is shown in Figure 6. The temperature distribution varies inversely with Pr It is clear that the temperature distribution decreases for a large Pr and increases for small values of Pr. Physically, the fluids with a small Pr have larger thermal diffusivity, and this effect

is opposite for a higher Prandtl number. Due to this fact, a large Pr causes the thermal boundary layer to decrease. The effect is even more distinct for a small Pr, since the thermal boundary layer thickness is relatively large. The impact of the thermal radiation parameter Rd is presented in Figure 7. Thermal radiation has a dominating role in the comprehensive surface heat transmission when the coefficient of convection heat transmission is small. When we increase the thermal radiation parameter Rd, we see that it augments the temperature in the boundary layer area in the fluid layer. Figure 8 represents the influence of κ on the velocity profile. It is noted that the increasing value of κ increases the velocity of the fluid during oscillation. The features of the porosity parameter κ on the velocity field are shown in Figure 9, and have an imperative character in terms of the flow motion. The higher values of κ increase the porous space; this produces resistance in the flow path and reduces the flow motion. In fact, growing values of γ show a large number of porous spaces, which create resistance in the flow path and reduce overall fluid motion. Figure 10 shows the influence of the dimensionless fluid parameter λ on the velocity profile. Large values of λ speed up the flow motion and increase its oscillation. Figure 11 presents the influence of the heat source/sink γ on the temperature profile. It is obvious from the figure that increases in the value enhance the temperature profile γ of the flow. This occurs due to the fact that the different values of γ perform like a heat generator, releasing heat energy to the flow. This helps to develop the thermal boundary layer thickness. Figures 12 and 13 show the effect of different values of τ on the velocity and temperature profiles. Greater values of τ increase the temperature and velocity profiles.

Figures 14 and 15 show the comparison between HAM and numerical solutions using the ND-solve technique on velocity and temperature profiles, respectively. An excellent agreement was found between the homotopy analysis method and the ND-solve technique.
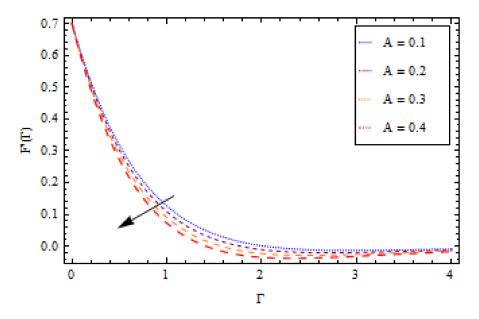

Figure 4. Impact of A on velocity profile $F'(\Gamma)$ when $Pr = 0.5$, $K = 0.5$, $Rd = 0.5$, $\lambda = 0.5$, $\kappa = 0.5$, $\gamma = 0.5$, $Sin\tau = 1.0$.
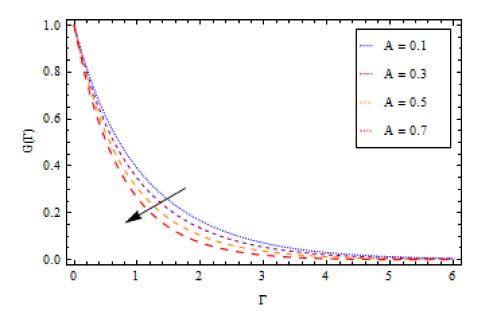
Figure 5. Impact of *A* on temperature profile $G(\Gamma)$, when $Pr = 0.5$, $K = 0.5$, $Rd = 0.5$, $\lambda = 0.5$, $\kappa = 0.5$, $\gamma = 0.5$, $\text{Sin}\tau = 1.0$.
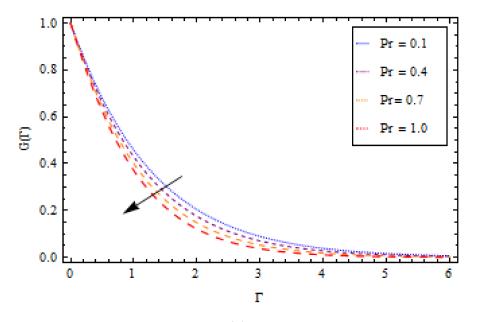

Figure 6. Impact of *Pr* on temperature profile $G(\Gamma)$, when $A = 0.5$, $K = 0.5$, $Rd = 0.5$, $\lambda = 0.5$, $\kappa = 0.5$, $\gamma = 0.5$, $\text{Sin}\tau = 1.0$.
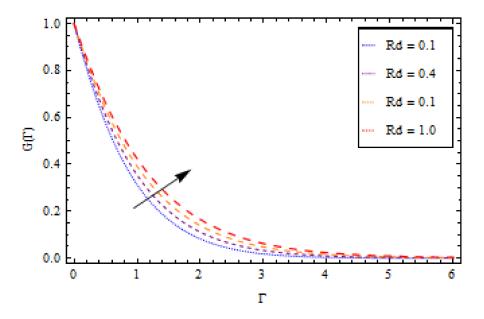
Figure 7. Impact of Rd on temperature profile $G(\Gamma)$, when $K = 0.5$, $Pr = 0.5$, $\lambda = 0.5$, $\kappa = 0.5$, $\gamma = 0.5$, $\mathrm{Sin}\tau = 1.0$, $A = 0.5$.

Figure 8. Impact of K on velocity profile $F'(\Gamma)$, when $Pr = 0.5$, $Rd = 0.5$, $\lambda = 0.5$, $\kappa = 0.5$, $\gamma = 0.5$, $\mathrm{Sin}\tau = 1.0$, $A = 0.5$.
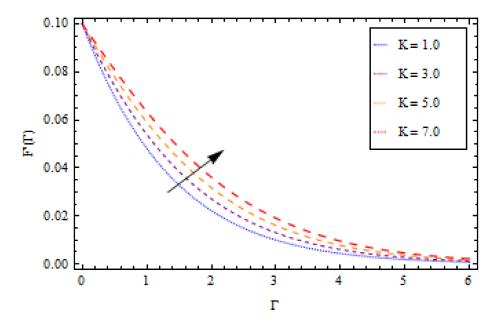
Figure 9. Impact of κ on velocity profile $F'(\Gamma)$, when $Pr = 0.5$, $Rd = 0.5$, $\lambda = 0.5$, $\kappa = 0.5$, $\gamma = 0.5$, $Sin\tau = 1.0$, $A = 0.5$.
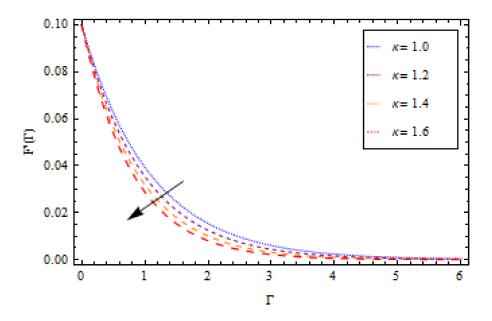

Figure 10. Impact of λ on velocity profile $F'(\Gamma)$ when $Pr = 0.5$, $Rd = 0.5$, $K = 0.5$, $\kappa = 0.5$, $\gamma = 0.5$, $Sin\tau = 1.0$, $A = 0.5$.
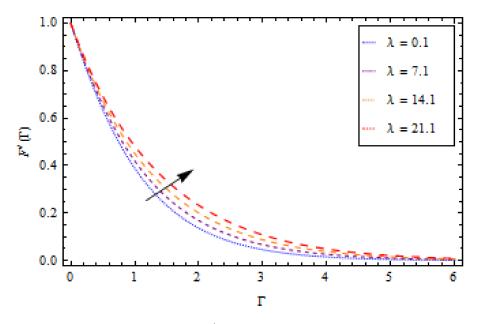
Figure 11. Impact of γ on temperature profile $G(\Gamma)$, when $Pr = 0.5$, $Rd = 0.5$, $K = 0.5$, $\kappa = 0.5$, $\lambda = 0.5$, $\mathrm{Sin}\tau = 1.0$, $A = 0.5$.

Figure 12. Impact of τ on velocity profile $F'(\Gamma)$, when $Pr = 0.5$, $Rd = 0.5$, $K = 0.5$, $\kappa = 0.5$, $\gamma = 0.5$, $\lambda = 0.5$, $A = 0.5$.
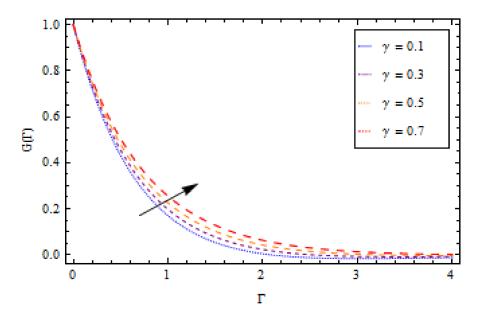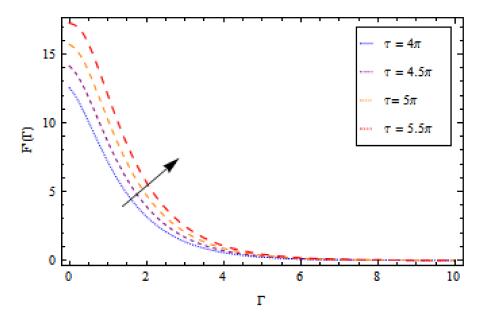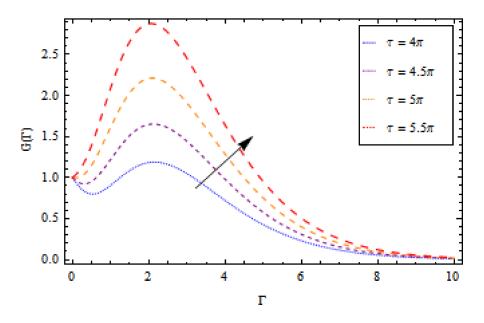
Figure 13. Impact of τ on temperature profile $G(\Gamma)$, when $Pr = 0.5$, $Rd = 0.5$, $K = 0.5$, $\kappa = 0.5$, $\gamma = 0.5$, $\lambda = 0.5$, $A = 0.5$.
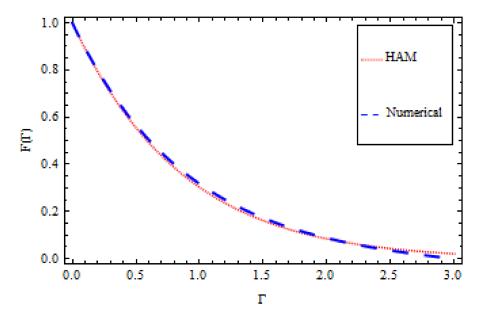

Figure 14. HAM and numerical comparison for velocity profile $F'(\Gamma)$.
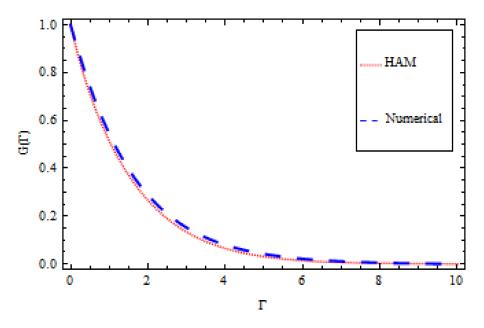
Figure 15. HAM and numerical comparison for temperature profile $G(\Gamma)$.

Table Discussion

The physical quantities such as the skin friction coefficient C_f and heat flux Nu, which are of engineering interest, are calculated through Tables 1 and 2. The impact of κ, K and λ on the skin friction coefficient is shown in Table 1. It is observed that higher values of κ, K and λ reduce the coefficient. The impact of Pr, γ and Rd on heat flux is shown in Table 2. It is observed that higher values of Pr decrease the heat flux, while higher values of γ and Rd increase the heat flux. The comparison of HAM and the numerical solution and the absolute error are provided in Tables 3 and 4. Table 3 shows the comparison of HAM and the numerical solution for the velocity profile, while Table 4 shows the comparison of HAM and the numerical solution for the temperature profile.

Table 1. The numerical values of skin fraction $(1 + K)F''(0) - \frac{K}{3}\Psi(F''(0))$, when $A = 0.5$, $\Psi = 1$ at time instant $\tau = \pi/2$.

κ	K	λ	C_f
0.5	-	-	−1.29447
0.7	-	-	−1.39927
0.9	-	-	−1.50053
1.1	1.0	-	−1.59913
-	1.3	-	−1.68426
-	1.5	-	−1.73747
-	1.7	0.5	−1.78810
-	-	0.6	−1.81316
-	-	0.7	−1.84069

Table 2. The numerical values of heat flux $\left(1 + \frac{4}{3}Rd\right)G'(0)$, when $A = 0.5$, $\Psi = 1$ at time instant $\tau = \pi/2$.

Pr	γ	Rd	Nu_x
1.0	-	-	1.82770
1.2	-	-	1.80574
1.4	-	-	1.78404
1.6	2.5	-	1.76259
-	2.6	-	1.79740
-	2.7	-	1.83133
-	2.8	0.3	1.85965
-	-	0.4	1.97571
-	-	0.5	2.08693

Table 3. The association between HAM and numerical solution for $F'(\Gamma)$, when $K = 0$, $A = 0.2$, $\kappa = 0.5$, $Rd = 1.0$, $\mathrm{Sin}\tau = 1.0$, $\lambda = Pr = \gamma = 0.6$.

Γ	HAM Solution $F'(\Gamma)$	Numerical Solution $F'(\Gamma)$	Absolute Error AE
0.0	1.12757×10^{-17}	0.000000	1.12757×10^{-17}
0.5	0.378563	0.381439	0.002876
1.0	0.586888	0.596535	0.009647
1.5	0.699341	0.715829	0.016488
2.0	0.758826	0.779103	0.020276
2.5	0.789566	0.808656	0.019089
3.0	0.804988	0.816817	0.011828
3.5	0.812414	0.866641	0.054227
4.0	0.815772	0.873029	0.057257
4.5	0.817129	0.875971	0.058842
5.0	0.817552	0.876772	0.059220

Table 4. The association between HAM and numerical solution for $G(\Gamma)$, when $K = 0$, $A = 0.2$, $\kappa = 0.5$, $Rd = 1.0$, $\mathrm{Sin}\tau = 1.0$, $\lambda = Pr = \gamma = 0.6$.

Γ	HAM Solution $G(\Gamma)$	Numerical Solution $G(\Gamma)$	Absolute Error AE
0	1.000000	1.000000	0.000000
1.0	0.513778	0.543757	0.029978
2.0	0.266242	0.288424	0.022182
3.0	0.133781	0.152038	0.018257
4.0	0.065247	0.080017	0.014769
5.0	0.030998	0.042041	0.011042
6.0	0.014391	0.021973	0.007582
7.0	0.006548	0.011297	0.004748
8.0	0.002927	0.005503	0.002575
9.0	0.001288	0.002181	0.000892
10.0	0.000559	2.093×10^{-6}	0.000557

6. Conclusions

In this article, we analyzed an Eyring–Powell fluid over an oscillatory thermally conductive stretching sheet in the presence of thermal radiation and a heat source/sink. A coordinate transformation was used to transform the semi-infinite flow domain to a finite computational domain. The homotopy analysis method was used to solve the modeled problem. The main remarks from this study are as follows:

- The amplitude of the velocity decreased with an increase in A and porosity κ, while it increased with an increase in the dimensionless fluid parameters K and λ.
- The temperature increased with an increase in A, the radiation parameter Rd, and the heat source/sink γ, while it decreased with an increase in the Prandtl number Pr and the ratio of the oscillation frequency of the sheet to its stretching rate A.
- The local Nusselt number increased with an increase in the Prandtl number Pr, the heat source/sink γ, the dimensionless fluid parameter K and the radiation parameter Rd, while it decreased with an increase in the porosity κ and the dimensionless fluid parameter λ.

Author Contributions: Abdullah and Zahir Shah modelled the problem. Waris Khan solved the problem. Abdullah and Muhammad Idrees wrote the manuscript. Zahir Shah and Saeed Islam thoroughly checked the mathematical modeling and English language corrections. Saeed Islam and Taza Gul contributed in the results and discussions. All the corresponding authors finalized the manuscript after its internal evaluation.

Nomenclature

P	pressure (Pa)
c	constant
X,Y	topological space
x,y	coordinates
$\vec{u}, \vec{v}$	velocity components (ms^{-1})
C_p	specific heat $\left(\frac{\text{J}}{\text{kgK}}\right)$
Ψ, Y	fluid materials
Q_0	heat source/sink
k	thermal conductivity $(\text{Wm}^{-1}\text{K}^{-1})$
Q_{rad}	radiative heat flux $\left(\text{Wm}^{-2}\right)$
k'	absorption coefficient
K	fluid parameter
A	ratio of the oscillation frequency
Rd	radiation parameter
Pr	Prandtl number
C_f	skin fraction coefficient
Nu_x	local Nusselt number
Greek Letters	
μ	dynamic viscosity (mPa)
v	constant
v	kinematic viscosity (m^2/s)
ρ	density (kg/m^3)
σ'	Stefan–Boltzmann constant
κ	porosity term
γ	heat source/sink

References

1. Sakiadis, B.C. Boundary Layer Behavior on Continuous Solid Surfaces: II Boundary Layer on a Continuous Flat Surface. *AIChE J.* **1961**, *7*, 221–225. [CrossRef]
2. Crane, L.J. Flow past a stretching plate. *Z. Angew. Math. Phys.* **1970**, *21*, 645–647. [CrossRef]
3. Gupta, P.S.; Gupta, A.S. Heat and mass transfer on stretching sheet with suction or blowing. *Can. J. Chem. Eng.* **1977**, *55*, 744–746. [CrossRef]
4. Anderson, H.I.; Hansen, O.R.; Olmedal, B. Diffusion of chemically reactive species from a stretching sheet. *Int. J. Heat Mass Transf.* **1994**, *37*, 659–664. [CrossRef]
5. Pop, I.; Na, T.Y. Unsteady flow past a stretching sheet. *Mech. Res. Commun.* **1996**, *23*, 413–422. [CrossRef]
6. Cortell, R. A note on flow and heat transfer of viscoelastic fluid over a stretching sheet. *Int. J. Non-Lin. Mech.* **2006**, *41*, 78–85. [CrossRef]
7. Ariel, P.D. Axismmetric flow of a second grade fluid past a stretching sheet. *Int. J. Eng. Sci.* **2001**, *39*, 529–553. [CrossRef]
8. Rashdi, M.M.; Ali, M.E.S.; Yang, Z. Entropy generation on MHD Eyring–Powell nanofluid through a permeable stretching surface. *Entropy* **2016**, *18*, 224. [CrossRef]
9. Rashdi, S.; Esfahani, A.J.; Ellahi, R. Convective heat transfer and particle motion in an obstructed duct with two side-by-side obstacles by means of DPM model. *Appl. Sci.* **2017**, *7*, 431. [CrossRef]
10. Hayat, T.; Abbas, Z.; Sajid, M. Heat and mass transfer analysis on the flow of second grade fluid in the presence of chemical reaction. *Phys. Lett. A* **2008**, *372*, 2400–2408. [CrossRef]
11. Hayat, T.; Sajid, M. Analytic solution for axisymmetric flow and heat transfer flow of a second grade fluid past a stretching sheet. *Int. J. Heat Mass Transf.* **2007**, *50*, 75–84. [CrossRef]
12. Hayat, T.; Asad, S.; Mustafa, M.; Alsaedi, A. Radiation effects on the flow of Powell–Eyring fluid past an unsteady inclined stretching sheet with Non-uniform heat source/sink. *PLoS ONE* **2014**, *9*, e103214. [CrossRef] [PubMed]

13. Hayat, T.; Awais, M.; Asghar, S. Radiative effects in a three-dimensional flow of MHD Eyring–Powell fluid. *J. Egypt. Math. Soc.* **2013**, *21*, 379–384. [CrossRef]

14. Powell, R.E.; Eyring, H. Mechanism for the Relaxation Theory of Viscosity. *Nature* **1944**, *154*, 427–428. [CrossRef]

15. Prasad, K.V.; Datti, P.S.; Raju, B.T. Momentum and Heat Transfer of a Non-Newtonian Eyring–Powell Fluid over a Non-Isothermal Stretching Sheet. *Int. J. Math. Arch.* **2013**, *4*, 230–241.

16. Noreen, S.; Qasim, M. Peristaltic Flow of MHD Eyring–Powell Fluid in a Channel. *Eur. Phys. J. Plus* **2013**, *128*, 91–103. [CrossRef]

17. Ellahi, R. Numerical study of magnetohydrodynamics generalized Couette flow of Eyring–Powell fluid with heat transfer and slip condition. *Int. J. Numer. Methods Heat Fluid Flow* **2016**, *26*, 1433–1445. [CrossRef]

18. Ellahi, R.; Hassan, M.; Zeeshan, A. Shape effects of spherical and nonspherical nanoparticles in mixed convection flow over a vertical stretching permeable sheet. *J. Mech. Adv. Mater. Struct.* **2017**, *24*, 1231–1238. [CrossRef]

19. Mahmoudi, M.A.A.; Ahmad, M.; Megahed, M. Slip flow of Powell–Eyring liquid film due to an unsteady stretching sheet with heat. *Braz. J. Phys.* **2016**, *3*, 299–307. [CrossRef]

20. Zaman, H.; Shah, M.A.; Ibrahim, M. Unsteady incompressible coquette flow problem for the Eyring–Powell Model with porous walls. *Am. J. Comput. Math.* **2013**, *3*, 313–325. [CrossRef]

21. Hayat, T.; Tanveer, A.; Yasmin, H.; Alsaedi, A. Effects of convective conditions and chemical reaction on peristaltic flow of Erying–Powell fluid. *Appl. Bionics Biomech.* **2014**, *11*, 221–233. [CrossRef]

22. Javed, T.; Ali, N.; Abbas, Z.; Sajid, M. Flow of an Eyring–Powell non-Newtonian over a stretching sheet. *Chem. Eng. Commun.* **2012**, *200*, 327–336. [CrossRef]

23. Hayat, T.; Imtiaz, M.; Alsaedi, A. Effects of homogeneous-heterogeneous reactions in flow of Powell–Eyring fluid. *J. Cent. South. Univ. Technol.* **2015**, *22*, 3211–3216. [CrossRef]

24. Khan, N.A.; Sultan, F. On the double diffusive convection flow of Eyring–Powell fluid due to cone through a porous medium with Soret and Dufour effects. *AIP ADVANCES* **2015**, *5*, 057140. [CrossRef]

25. Panigrahi, S.; Reza, M.; Mishra, A.K. Mixed convective flow of a Powell–Eyring fluid over non-linear stretching surface with thermal diffusion and diffusion thermo. *Procedia Eng.* **2015**, *127*, 645–651. [CrossRef]

26. Tawadem, L.M.; Gmetri, P.; Koti, A. Thin film flow and heat transfer over an unsteady stretching sheet with thermal radiation, internal heating in presence of external magnetic field. *Int. J. Adv. Appl. Math. Mech.* **2016**, *3*, 29–40.

27. Ellahi, R.; Tariq, M.H.; Hassan, M.; Vafai, K. On boundary layer magnetic flow of nano-Ferroliquid under the influence of low oscillating over stretchable rotating disk. *J. Mol. Liq.* **2017**, *229*, 339–345. [CrossRef]

28. Zeeshan, A.; Majeed, A.; Ellahi, R. Effect of magnetic dipole on viscous ferro-fluid past a stretching surface with thermal radiation. *J. Mol. Liq.* **2016**, *215*, 549–554. [CrossRef]

29. Maqbool, M.; Sohail, A.; Naeema, M.; Ellahi, R. Hall effect on Falkner-Skan boundary layer flow of FENE-P fluid over a stretching sheet. *Commun. Theor. Phys.* **2016**, *66*, 547–554. [CrossRef]

30. Shirvan, M.K.; Ellahi, R.; Mirzakhanlar, S.; Mamourian, M. Enhancement of Heat Transfer and Heat Exchanger Effectiveness in a Double Pipe Heat Exchanger Filled with Porous Media: Numerical Simulation and Sensitivity Analysis of Turbulent Fluid Flow. *Appl. Therm. Eng.* **2016**, *109*, 761–774. [CrossRef]

31. Ramesh, G.K.; Prasannakumara, B.C.; Gireesha, B.J.; Rashidi, M.M. Casson Fluid Flow near the Stagnation Point over a Stretching Sheet with Variable Thickness and Radiation. *J. Appl. Fluid Mech.* **2016**, *9*, 1115–1122. [CrossRef]

32. Krishnamurthy, M.R.; Gireesha, B.J.; Prasannakumara, B.C.; Gorla, R.S.R. Thermal radiation and chemical reaction effects on boundary layer slip flow and melting heat transfer of nanofluid induced by a nonlinear stretching sheet. *Nonlinear Eng.* **2016**, *5*, 147–159. [CrossRef]

33. Prasannakumara, B.C.; Gireesha, B.J.; Gorla, R.S.R.; Krishnamurthy, M.R. Effect of multiple slips and thermal radiation on MHD flow of Jeffery nanofluid with heat transfer. *J. Nanofluids* **2016**, *5*, 82–93. [CrossRef]

34. Prasannakumara, B.C.; Gireesha, B.J.; Gorla, R.S.R.; Krishnamurthy, M.R. Non-Linear Thermal Radiation and Slip Effect on Boundary Layer Flow and Heat Transfer of Suspended Nanoparticles over a Stretching Sheet Embedded in Porous Medium with Convective Boundary Conditions. *J. Nanofluids* **2016**, *5*, 522–530.

35. Bakier, A.Y. Thermal radiation effect on mixed convection from vertical surface in saturated porous media. *Int. Commun. Heat Mass Transf.* **2001**, *28*, 119–126. [CrossRef]

36. Moradi, A.; Ahmadikia, H.; Hayat, T.; Alsaedi, A. On mixed convection-radiation interaction about an inclined plate through a porous medium. *Int. J. Therm. Sci.* **2013**, *64*, 129–136. [CrossRef]

37. Chaudhary, S.; Singh, S.; Chaudhary, S. Thermal radiation effects on MHD Boundary layer flow over an exponentially stretching surface. *Sci. Res. Publ. Appl. Math.* **2015**, *6*, 295–303. [CrossRef]

38. Liao, S.J. The Proposed Homotopy Analysis Method for the Solution of Nonlinear Problems. Ph.D. Thesis, Shanghai Jiao Tong University, Shanghai, China, 1992.

39. Liao, S.J. An Explicit, Totally Analytic Approximate Solution for Blasius Viscous Flow Problems. *Int. J. Non-Linear Mech.* **1999**, *34*, 759–778. [CrossRef]

40. Liao, S.J. *Beyond Perturbation: Introduction to the Homotopy Analysis Method*; Chapman and Hall, CRC: Boca Raton, FL, USA, 2003.

41. Rashidi, M.M.; Siddiqui, A.M.; Asadi, M. Application of homotopy analysis method to the unsteady squeezing flow of a second grade fluid between circular plates. *Math. Probl. Eng. Art.* **2010**. [CrossRef]

42. Rashidi, M.M.; Pour, S.A.M. Analytic approximate solutions for unsteady boundary-layer flow and heat transfer due to a stretching sheet by homotopy analysis method. *Nonlinear Anal. Model. Control* **2010**, *15*, 83–95.

43. Abbasbandy, S. Homotopy analysis method for heat radiation, equations. *Int. Commun. Heat Mass Transf.* **2007**, *34*, 380–388. [CrossRef]

44. Nadeem, S.; Awais, M. Thin film flow of an unsteady shrinking sheet through porous medium with variable viscosity. *Phys. Lett. A* **2008**, *372*, 4965–4972. [CrossRef]

45. Khan, S.U.; Ali, N.; Abas, Z. Hydromagnetic Flow and Heat Transfer of Eyring–Powell Fluid over an Oscillatory Stretching Sheet with Thermal Radiation. *Appl. Appl. Math.* **2015**, *10*, 893–908.

46. Shah, Z.; Gul, T.; Khan, A.M.; Ali, I.; Islam, S. Effects of hall current on steady three dimensional non-newtonian nanofluid in a rotating frame with brownian motion and thermophoresis effects. *J. Eng. Technol.* **2017**, *6*, 280–296.

47. Shah, Z.; Islam, S.; Gul, T.; Bonyah, E.; Khan, M.A. The electrical MHD and hall current impact on micropolar nanofluid flow between rotating parallel plates. *Results Phys.* **2018**. [CrossRef]

48. Hammed, H.; Haneef, M.; Shah, Z.; Islam, S.; Khan, W.; Muhammad, S. The Combined Magneto hydrodynamic and electric field effect on an unsteady Maxwell nanofluid Flow over a Stretching Surface under the Influence of Variable Heat and Thermal Radiation. *Appl. Sci.* **2018**, *8*, 160. [CrossRef]

49. Muhammad, S.; Ali, G.; Shah, Z.; Islam, S.; Hussain, A. The Rotating Flow of Magneto Hydrodynamic Carbon Nanotubes over a Stretching Sheet with the Impact of Non-Linear Thermal Radiation and Heat Generation/Absorption. *Appl. Sci.* **2018**, *8*, 482. [CrossRef]